Heliyon 10 (2024) e29598

Contents lists available at ScienceDirect

Heliyon

journal homepage: www.cell.com/heliyon

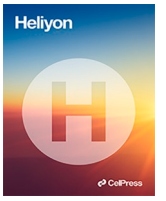

Research article

Microbiome profiling and Co-metabolism pathway analysis in cervical cancer patients with acute radiation enteritis

Chen-ying Ma [a], Jing Zhao [a], Ju-ying Zhou [a,b,*]

[a] Department of Radiation Oncology, the First Affiliated Hospital of Soochow University, Suzhou, 215006, China
[b] State Key Laboratory of Radiation Medicine and Protection, Soochow University, Suzhou, 215123, China

ARTICLE INFO

Keywords:
Cervical cancer
Acute radiation enteritis
Gut microbiota
Metabonomics
Biomarker

ABSTRACT

Background: Intestinal bacteria significantly contribute to the metabolism of intestinal epithelial tissues. As the occurrence and development of radiation enteritis (RE) depend on the "co-metabolism" microenvironment formed by the host and intestinal microbiota, which involves complex influencing factors and strong correlations, ordinary techniques struggle to fully explain the underlying mechanisms. However, given that it is based on systems biology, metabolomics analysis is well-suited to address these issues. This study aimed to analyze the metabolomic changes in urine, serum, and fecal samples during volumetric modulated arc therapy (VMAT) for cervical cancer and screen for characteristic metabolites of severe acute radiation enteritis (SARE) and RE.

Methods: We enrolled 50 patients who received radiotherapy for cervical cancer. Urine, serum, and fecal samples of patients were collected at one day before radiotherapy and the second week, fourth week, and sixth week after the start of radiotherapy. Control group samples were collected during the baseline period. Differential metabolites were identified by metabolomics analysis; co-metabolic pathways were clarified. We used the mini-SOM library for incorporating characteristic metabolites, and established metabolite classification models for predicting SARE and RE.

Results: Urine and serum sample data showed remarkable clustering effect; metabolomics data of the fecal supernatant were evidently disturbed. Patient sample analyses during VMAT revealed the following. *Urine samples*: Downregulation of the pyrimidine and riboflavin metabolism pathways as well as initial upregulation followed by downregulation of arginine and proline metabolism pathways and the arginine biosynthesis pathway. *Fecal samples*: Upregulation of linoleic acid and phenylalanine metabolic pathways and initial downregulation followed by upregulation of arachidonic acid (AA) metabolic pathways. *Serum samples*: Initial upregulation followed by downregulation of the arginine biosynthesis pathway and downregulation of glutathione, AA, and arginine and proline metabolic pathways.

Conclusion: Patients with cervical cancer exhibited characteristic metabolic pathways and characteristic metabolites predicting RE and SARE were screened out. An effective RE mini-SOM classification model was successfully established.

* Corresponding author. Department of Radiation Oncology, the First Affiliated Hospital of Soochow University, No.188 Shizi Street, Suzhou, 215123, China.

E-mail addresses: machenying@suda.edu.cn (C.-y. Ma), zhaojing850109@163.com (J. Zhao), zhoujuyingsy@163.com (J.-y. Zhou).

https://doi.org/10.1016/j.heliyon.2024.e29598
Received 6 September 2023; Received in revised form 7 April 2024; Accepted 10 April 2024

1. Background

Intestinal bacteria contribute significantly to the metabolism of intestinal epithelial tissue. Constructing a new gut microbiota manipulation strategy that targets specific gut microbiota and their metabolites may reduce adverse reactions and improve response to anti-tumor therapy. We herein investigated the molecular mechanisms underlying gut microbiota coexistence in radiation enteritis (RE) and screened for relevant biomarkers using metabolomics analysis. This work is presently still in the preliminary exploration stage.

Guo et al. [1] believe that the functional roles of microorganisms in nature often rely on the "co-metabolism" of multiple bacterial species. In more complex organisms, such as the human body, the metabolic products generated by symbiotic microorganisms can be transmitted to and can affect every cell [2]. Under normal physiological conditions, gut microbiota play a regulatory role in several pathways, such as protein–peptide–amino acid metabolism, carbohydrate metabolism, vitamin and trace element metabolism, bile acid–cholesterol metabolism, and hormone metabolism. Cheng et al. [3] have made efforts to model the human gut microbiome in mice yielding crucial insights into the mechanisms underlying host-microbe interactions. The research revealed that mice colonized by either hCom2 or a human fecal community exhibit similar phenotypes, suggesting that this consortium will enable a mechanistic interrogation of species and genes in microbiome-associated phenotypes. Singh et al. [4] confirmed that the metabolic abnormalities in urine and plasma of animal models receiving total body irradiation were mainly caused by the combined effect of the host and intestinal microbial communities. This indicates that radiation changes the normal physiological function of the intestinal microbiota, as reflected in changes in body metabolites. Li et al. [5] demonstrated that changes in metabolites in body fluids, such as plasma or urine, may effectively explain how the body comprehensively responds to radiation effects, and therefore, these are considered a new type of biological marker of radiation damage.

Therefore, it is believed that understanding radiation-caused abnormalities in body metabolites can reveal the host–microbe interaction mechanism during radiation injury, identify specific metabolic molecules, and consequently help achieve early, more direct, rapid, and accurate clinical diagnosis and prognosis assessment of radiation exposure.

This study highlights significant changes in metabolic pathways in urine, fecal, and serum samples of cervical cancer patients undergoing volumetric modulated arc therapy (VMAT). These include the downregulation of pyrimidine and riboflavin metabolism in urine and upregulation of linoleic acid and phenylalanine pathways in fecal samples. Such insights can help clinicians understand the metabolic impact of VMAT on patients, thus enabling more informed and targeted interventions. The identification of characteristic metabolites that predict RE and SARE is a crucial step forward. By monitoring these metabolites, healthcare providers can potentially predict the onset and severity of RE and SARE in patients undergoing radiotherapy. This prediction capability can help establish proactive management strategies to mitigate these conditions. By understanding each patient's unique metabolic response to radiotherapy, clinicians can tailor treatment plans to better suit individual needs, thus potentially enhancing treatment efficacy while minimizing adverse effects. Metabolite classification models make early intervention and more effective management of RE and SARE possible. This approach can significantly improve patient outcomes by addressing these complications promptly and effectively.

This study provides valuable insights into the metabolic changes associated with radiotherapy in cervical cancer patients and introduces an innovative approach for predicting and managing RE and SARE. These findings can significantly enhance patient care by enabling personalized treatment strategies and improving the management of radiotherapy-induced complications.

2. Methods

2.1. Patient selection

Herein, we selected 50 patients with cervical cancer who received pelvic local radiotherapy between August 2017 and August 2018 at the Department of Radiation Oncology of The First Affiliated Hospital of Soochow University. The following were the inclusion criteria: (1) pathologically confirmed cervical cancer; (2) age: 18–80 years; (3) good understanding and communication skills; and (4) absence of any history of intestinal or metabolic diseases. The exclusion criteria were as follows: (1) refusal to participate in the study; (2) treatment termination owing to serious complications during and/or after radiotherapy (e.g., severe infection, massive hemorrhage, severe bone marrow suppression, vaginovesical fistula, vaginorectal fistula, and cardiopulmonary, hepatic, and renal insufficiencies); and (3) severe heart, liver, and kidney dysfunction.

This study was approved by the medical ethics committee of The First Affiliated Hospital of Soochow University [approval No. 2016 (100)]. Signed informed consent was obtained from all participants.

2.2. Treatment

Depending on the International Federation of Gynecology and Obstetrics (FIGO) stage of the patient, radiotherapy was combined with hyperthermia or chemotherapy for each patient [6]. Patients with small tumors (FIGO stage $\leq$ IB_2) were treated only with postoperative adjuvant radiotherapy. Conversely, patients with more severe disease received concurrent chemoradiation (5 cycles of cisplatin 40 mg/m^2 body surface). If cisplatin was contra-indicated carboplatin was considered [7]. Patients with any combination of large nodal disease, very bulky tumors, and para-aortic nodal disease were given concurrent chemotherapy (cisplatin 70 mg/m^2 body surface, given in six schedules) before radiotherapy. We used the Monaco treatment planning system for designing the seven-field reverse dynamic VMAT plan with the use of unified parameters. Furthermore, for plan selection, daily cone beam computed tomography (CT) scan was used. In cases of extended-field irradiation, all patients received 50.4 Gy in 28 fractions or 45 Gy in 25

fractions. The administration of CT-guided high-dose-rate brachytherapy was done across four applications (6.5 Gy). If pathological lymph nodes were noted, a nodal boost was given (56 Gy/28f). The overall treatment time was kept under 7 weeks intentionally.

2.3. Data collection of acute RE

The monitoring of adverse reactions of all patients was performed at baseline and at 2 weeks, 4 weeks, and 6 weeks after radiotherapy initiation. Adverse reactions included abdominal pain, diarrhea, anal pain, bone marrow suppression, and hematochezia. The diagnosis and classification of RE were done in accordance with the National Institutes of Health Common Adverse Events Evaluation Criteria (CTCAE 5.0).

The adverse reaction score was reflected using the severe acute radiation enteritis scoring system (SARE-SS) established by us. According to the system, SARE-SS (version 2.0) = the sum of CTCAE scores of abdominal pain + diarrhea + hematochezia + anal pain. A score of $\geq$3 indicated SARE. Based on clinical symptoms and changes in ancillary test findings, at least two experienced radiation oncologists established the diagnosis of SARE.

2.4. Biological sample collection

(1) Fecal sample collection: After voiding urine, feces were collected in a sputum basin covered with a disposable medical biological sample collection bag. A disposable sampling spoon was used to collect ~2 g of fresh fecal sample and transfer it into a 2-mL sterile cryovial. Each sample was aliquoted into 2–3 backup tubes and stored at −80 °C freezer. The corresponding fecal samples collected were labeled as F0, F2, F4, and Ff, and the control group was labeled as FCK.
(2) Urinary specimen collection: About 10 mL of the first morning urine (midstream urine) on an empty stomach was collected into a urine storage container. After centrifugation at 13,000*g* for 10 min and sediment removal, the supernatant was immediately frozen at −80 °C. The collected urine samples were labeled as U0, U2, U4, and Uf, and the control group was labeled as UCK.
(3) Peripheral venous blood sample collection: Herein, 5 mL of venous blood was collected under fasting condition, and the serum was separated by centrifugation at 13,000*g* for 2 min and immediately frozen and stored at −80 °C. The corresponding serum samples obtained were labeled as S0, S2, S4, and Sf, and the control group was labeled as SCK.
(4) The sampling time: one day before radiotherapy (T0), the second week after the start of radiotherapy (T2), the fourth week (T4), and at the end of radiotherapy, which is the sixth week (Tf).

2.5. Metabolite extraction

All samples were thawed at 4 °C, and 100 μL of extract was obtained from each sample and transferred to a 1.5-mL centrifuge tube. Then, after adding 400-μL methanol each tube one by one, the tubes were shaken for 60 s and the contents were mixed well. After centrifuging at 13,000*g* for 10 min at 4 °C, all of the fecal supernatant was collected and transferred to new centrifuge tubes for concentration and drying. 2-Chlorophenylalanine (20 ppm) was dissolved in 80 % methanol (150 μL), and the solution was filtered through a 0.22-μm membrane to obtain the test sample. Then, 20 μL of each test sample was mixed and placed in a quality control sample, and the remaining samples were detected using liquid chromatography/mass spectrometry.

2.6. Liquid chromatography/mass spectrometry-based untargeted metabolomics

Chromatographic conditions: (1) We used the Waters ACQUITY UPLC system with an ACQUITY UPLC® HSS T3 1.8 μm (2.1 mm × 150 mm) column. Notably, the automatic injector was set at 4 °C, with a column temperature of 40 °C and flow rate of 0.25 mL/min. The gradient elution volume was 5 μL, and the mobile phase comprised 0.1 % formic acid in both water (A) and acetonitrile (B). (2) Gradient elution was performed as follows: 0–1 min, 2 % B; 1.9–5 min, 2%–50 % B; 9.5–14 min, 50%–98 % B; 14–15 min, 98 % B; 15–15.5 min, 98%–2% B; and 15.5–17 min, 2 % B [8].

Mass spectrometry conditions: (1) Thermo LTQ Orbitrap XL was used with positive and negative ionization modes and an electrospray ionization source. These were set at 4.80 kV and 4.50 kV, respectively, with an auxiliary gas pressure of 15 arb and a sheath gas pressure of 45 arb. (2) The voltage was set at 35 V/-15 V, and the capillary temperature was maintained at 325 °C. The tube lens voltage was set at 50 V/-50 V; the resolution of full scan was 60,000 in the range of m/z 89–1000. The secondary fragmentation was performed by collision-induced dissociation (CID), and the collision voltage was 30 eV. The repeat count and the dynamic exclusion time were set to 2 and 15 s, respectively, which excluded unnecessary MS/MS information [9].

Sample pre-processing: Raw data were transformed to obtain retention time (rt), peak area (intensity), and mass-to-charge ratio (m/z) and to normalize the peak area to meet data comparison requirements at different scales.

Base peak chromatogram: The mass spectrometer continuously scans components from the red chromatographic flow and collects data, and the base peak chromatogram is obtained by continuously plotting the ion with the highest intensity in each mass spectrum.

2.7. Statistical analysis

This study used agglomerative hierarchical clustering for metabolite clustering analysis and orthogonal partial least squares discriminant analysis (OPLS-DA) for screening for metabolite biomarkers. The criteria for screening for differential metabolites were P value $\leq$ 0.05 and variable importance for the projection (VIP) $\geq$ 1, as determined using one-way analysis of variance with a P value of

≤0.05. The identification of differential metabolites was based on Metlin (http://metlin.scripps.edu), mzCloud (https://www.mzcloud.org), the HumanMetabolome Database (http://www.hmdb.ca), LipidMaps (http://www.lipidmaps.org), MassBank (http://www.massbank.jp/), and the Bionovogene self-built standard substance database. Differential metabolites were statistically analyzed using ROC curves, and box plots. The KEGG database was used for differential metabolite pathway analysis. Self-organizing maps (SOM) were used to predict metabolic molecule classification models for RE and SARE.

3. Results

3.1. Clinical characteristics of patients and VMAT-related acute RE

Among the 50 patients with cervical cancer included in this study, 35 patients were given postoperative adjuvant pelvic radiotherapy, 14 patients were given radical radiotherapy, and 1 patient was given pelvic radiotherapy along with after-loading vaginal radiotherapy because the tumor boundary and the vaginal margin were only 2 cm apart. The major adverse reactions associated with radiotherapy included abdominal pain, diarrhea, anal distension, bone marrow suppression, and hematochezia. All adverse reactions that occurred were grade 1–3, with no adverse reactions above grade 3. RE was noted in 42 cases (84 %), and SARE was noted in 15 cases (30 %). See Table 1 for the adverse reaction grading of acute RE.

3.2. The profile of biological metabolites in VMAT patients with cervical cancer

In this study, we used the second orthogonal component and first principal component to construct the OPLS-DA model (Fig. 1). Significant clustering effects were noted from serum (Fig. 1a&d) and urine (Fig. 1b&e) sample data, and metabolomics (Fig. 1c&f) data of the fecal supernatant were evidently disturbed. Potential differential metabolites were identified by a *P* value of ≤0.05 and VIP >1.

3.3. Study on the functional mechanism of gut microbiota in acute RE patients

Patients with cervical cancer have their own tumor metabolic phenotype. We analyzed the metabolomics information of 50 enrolled patients and defined their characteristic metabolic molecules from serum, urine, and fecal supernatant samples; we compared the findings with those of the healthy control group and identified their characteristic metabolic molecules from serum, urine, and fecal supernatant samples.

During the VMAT of patients with cervical cancer, urine samples first revealed initial upregulation followed by downregulation of the proline and arginine metabolism pathways and the arginine biosynthesis pathway; furthermore, they revealed the downregulation of pyrimidine and riboflavin metabolism pathways (Fig. 2A). Fecal supernatant samples revealed that arachidonic acid (AA) metabolic pathways were first upregulated and then downregulated (Fig. 2B); conversely, linoleic acid (LC) metabolic pathways and phenylalanine metabolism were found to be upregulated. The serum samples revealed initial upregulation followed by downregulation of the arginine biosynthesis pathway. Conversely, arginine and proline metabolic pathways, glutathione metabolic pathway, and AA metabolic pathway were downregulated (Fig. 2C).

The changes in specific amino acids and pyrimidine metabolic pathways in urine samples reflect the potential impact of cancer and radiation therapy on the body's metabolism. Specific lipid metabolic pathways in fecal supernatant samples indicate the response of the intestinal microbiota and its metabolic activity to radiation therapy. The unique changes in amino acid and lipid metabolism in serum samples may reveal alterations in the systemic metabolic state after the occurrence of RE. These findings provide important information for personalized treatment of patients with cervical cancer. By monitoring these metabolic markers, doctors can better understand patients' responses to VMAT and adjust treatment plans accordingly to optimize efficacy and reduce adverse effects. Furthermore, monitoring these metabolic changes may also assist in the early identification of potential complications caused by radiation therapy, allowing for timely intervention.

3.4. ROC curve analysis of metabolic characterization in RE/SARE patients

We identified characteristic metabolic molecules (e.g., hydroquinone, 4-hydroxyproline, fumaric acid, and cytosine in urine samples (Fig. 3a&d); AA, spermine, creatine, and fumaric acid in serum samples (Fig. 3b&e); and AA, LC, L-phenylalanine, phenylethylamine, and N-acetyl-L-phenylalanine in fecal supernatant samples (Fig. 3c&f)) for their capacity to distinguish RE or SARE and proceeded with further data processing for metabolic molecules with potential predictive value. We screened out the RE-predictive

Table 1
Grading of adverse reactions in acute RE.

Adverse reaction	Level 0	Level 1	Level 2	Level 3
Diarrhea	13 (26)	29 (58)	5 (10)	3 (6)
Abdominal pain	29 (58)	18 (36)	3 (6)	0 (0)
Anal pain	33 (66)	11 (22)	6 (12)	0 (0)
Hematochezia	35 (70)	15 (30)	0 (0)	0 (0)

RE:radiation enteritis.

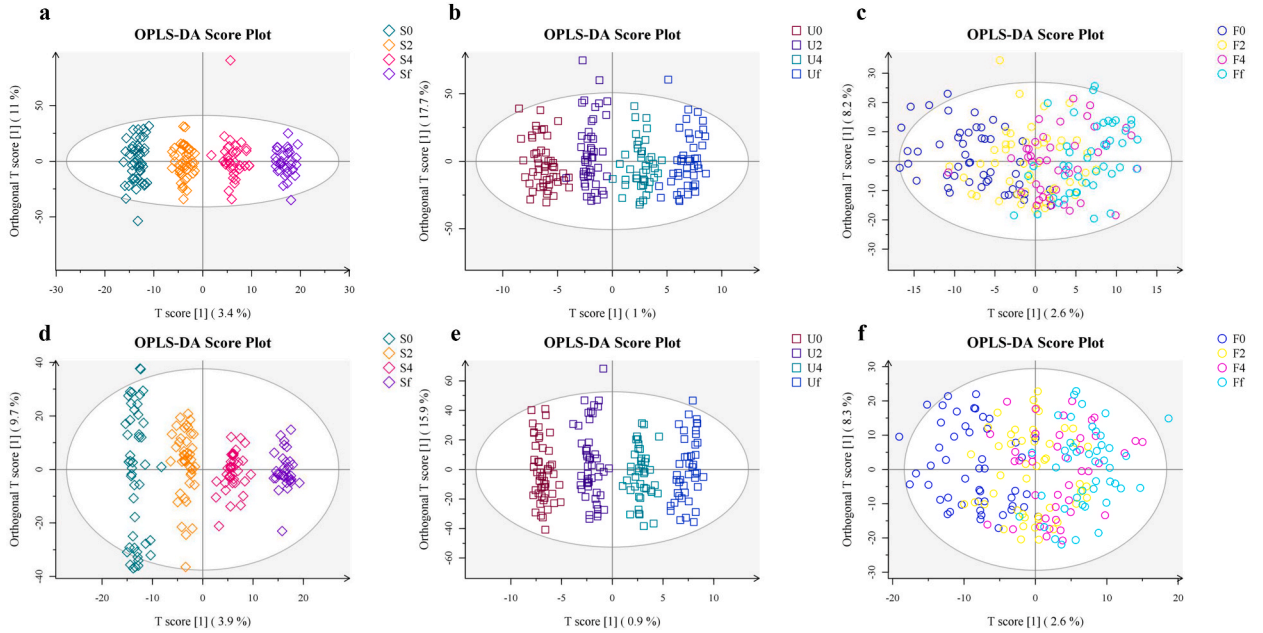

Fig. 1. The OPLS-DA score map of three types of biological samples during VMAT of patients with cervical cancer. (The four time points are T0, T2, T4, and Tf. a–c: The positive ion modes of peripheral blood (4231 precursor molecules), urine (3045 precursor molecules), and feces supernatant (2734 precursor molecules) samples, respectively; d-f; the negative ion modes of peripheral blood (3561 precursor molecules), urine (3521 precursor molecules), and feces supernatant (3036 precursor molecules) samples, respectively. We used the XCMS package of R (v3.3.2) for identification, filtration, and alignment of peaks. The main parameters were bw = 5, ppm = 15, peakwidth = c (10, 20), mzwid = 0.015, mzdiff = 0.01, and method = centWave. We obtained a data matrix including the mass-to-charge ratio (*m/z*), retention time, peak intensity, and other information and exported the data to excel for subsequent analysis. Batch normalization of peak areas was performed on the data to enable comparison of data of different magnitudes. Agglomerative hierarchical clustering for metabolite clustering analysis and orthogonal partial least squares discriminant analysis (OPLS-DA) were used to screen for metabolite biomarkers. The criteria for screening of differential metabolites were P value ≤ 0.05 and variable importance for the projection (VIP) ≥ 1, as determined using one-way analysis of variance with a P value of $\leq$0.05.).

metabolites, namely serum AA (AUC = 0.6322, $P = 0.002$), urinary hydroquinone (AUC = 0.6429, $P = 0.001$), and serum fumaric acid (AUC = 0.6399, $P = 0.001$), and SARE-predictive metabolites, namely fecal phenethylamine (AUC = 0.6193, $P = 0.016$) and urinary hydroquinone (AUC = 0.6866, $P = 0.002$; Fig. 3).

In clinical settings, these findings can be tremendously beneficial. For instance, the ability to use serum AA, urinary hydroquinone, and serum fumaric acid as predictors for RE and fecal phenethylamine and urinary hydroquinone as predictors for SARE allows for a more nuanced and precise approach to monitoring the health status of patients undergoing radiation therapy. The use of these metabolites as biomarkers could enable early detection and intervention, potentially reducing the severity of radiation-induced injuries. Furthermore, this approach can assist in tailoring individualized treatment plans based on the patient's metabolic response to radiation. It opens the door for personalized medicine, wherein treatments and monitoring strategies are optimized on the basis of the unique metabolic profile of each patient. This could lead to more effective treatment outcomes, with reduced adverse effects and improved quality of life for patients.

3.5. Correlation analysis between clinical factors and characteristic metabolites

We conducted a correlation analysis between clinical information (i.e., concurrent chemoradiotherapy, pathological classification, lymph node positivity, occurrence of RE, occurrence of SARE, age grouping, whether surgery was performed, whether extended field irradiation was given, whether baseline squamous cell carcinoma (SCC)-related antigen was elevated, risk stratification of cervical cancer, duration of radiotherapy, the age-adjusted Charlson Comorbidity Index score, and the FIGO stage) and characteristic metabolic molecules (i.e., hydroquinone, 4-hydroxyproline, fumaric acid, and cytosine in urine samples; AA, spermine, creatine, and fumaric acid in serum samples; and AA, LC, L-phenylalanine, phenylethylamine, and N-acetyl-L-phenylalanine in fecal supernatant samples).

According to cluster analysis findings, different pathological types affected the expression of pyrocatechol in urine, whereas whether or not surgery was performed and whether or not extended-field irradiation was received affected phenylethylamine expression in fecal supernatant samples. These variations in metabolic expression caused by treatment modalities and cancer pathology can inform personalized treatment strategies. Understanding how different treatments impact metabolic profiles can help clinicians tailor therapy to each patient's unique circumstances.

Different FIGO stages affected the expression of AA in the serum (Table 2). This implies that the severity and progression of cervical cancer, as indicated by FIGO staging, have a direct correlation with specific metabolic changes. Monitoring these metabolic markers

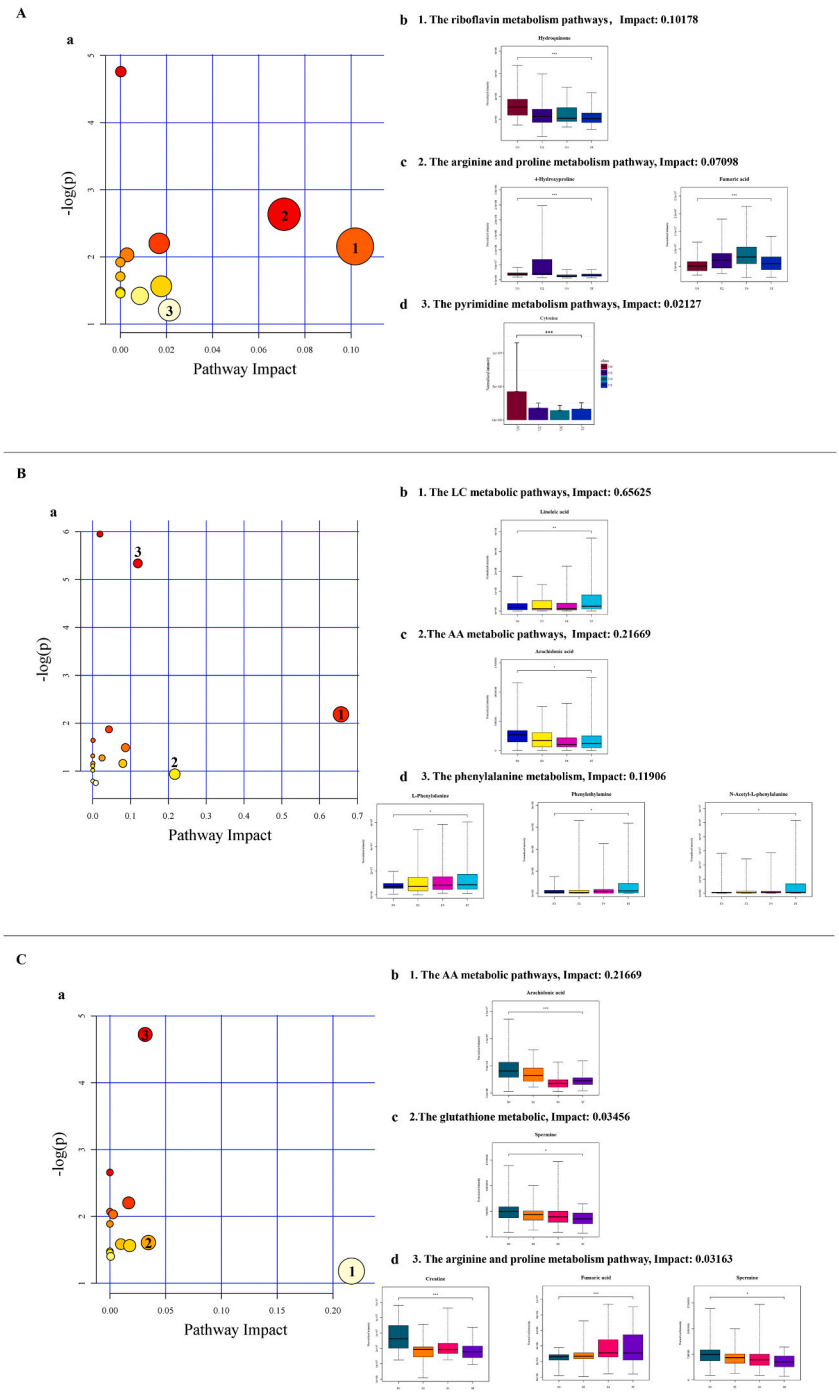

Fig. 2. A: Differentially altered metabolic pathways in urine samples during VMAT of patients with cervical cancer (a: pathway impact factor plot of urine samples, 1: the riboflavin metabolic pathway, 2: the arginine and proline metabolic pathways, 3: the pyrimidine metabolic pathway, and b–d: box plots of differential molecules in the top three metabolic pathways); B: Differentially altered metabolic pathways in fecal supernatant samples during VMAT of patients with cervical cancer (a: the pathway impact factor plot of fecal supernatant samples, 1: the fatty acid metabolism pathway, 2: the amino acid metabolism pathway, 3: the phenylalanine metabolism pathway, and b–d: box plots of differential molecules in the top three metabolic pathways); and C: Differentially altered metabolic pathways in serum samples during VMAT of patients with cervical cancer (a: pathway impact factor plot of peripheral blood samples, 1: the AA metabolic pathway, 2: the glutathione metabolic pathway, 3: arginine and proline metabolic pathways, and b–d: box plots of differential molecules in the top three metabolic pathways. Considering that this study involves four time periods, metabolite analysis used one-dimensional analysis of variance to further find differential metabolites. A P value of <0.05 indicated statistically significant difference. In the box plot of differential metabolites, P values < 0.05 and P values > 0.01 are represented by *, P values < 0.01 and P values > 0.001 are represented by **, and P values < 0.001 are represented by ***.).

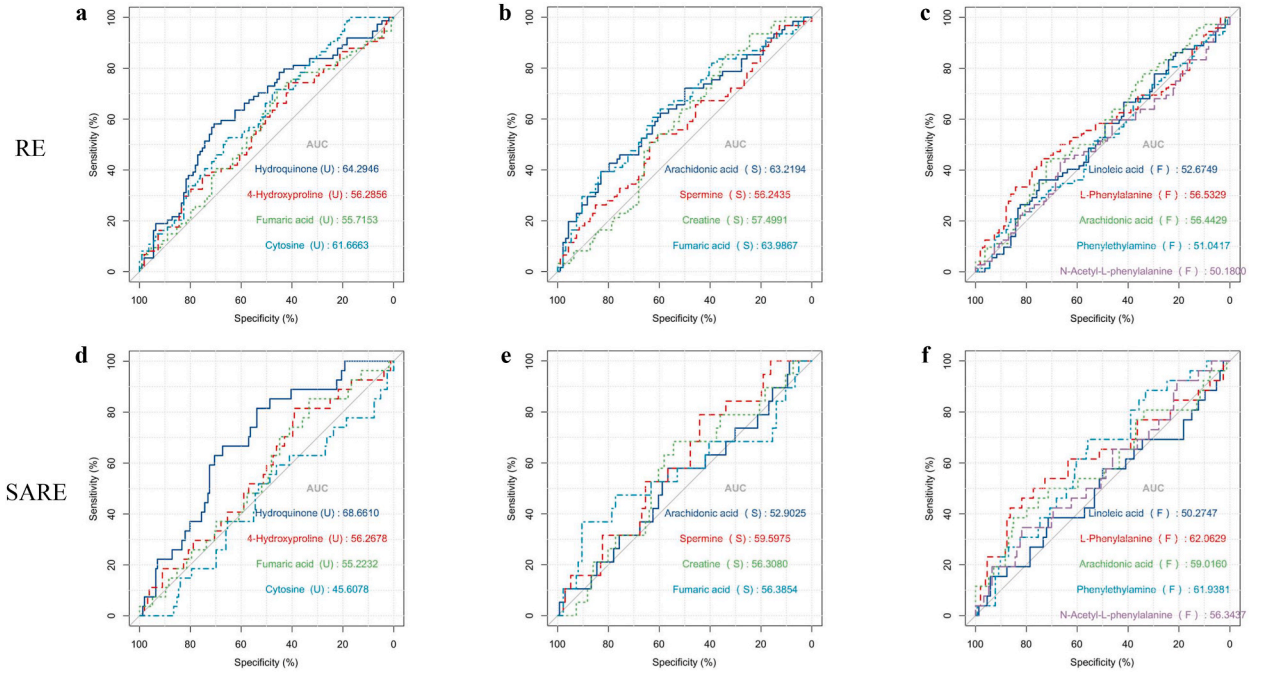

Fig. 3. ROC curves for identifying characteristic metabolic molecules predictive of RE and SARE. (a/d: urine sample, b/e: serum sample, c/f: fecal supernatant sample. The RE-predictive metabolites were serum AA (AUC = 0.6322, $P = 0.002$), urinary hydroquinone (AUC = 0.6429, $P = 0.001$), and serum fumaric acid (AUC = 0.6399, $P = 0.001$), and SARE-predictive metabolites were fecal phenethylamine (AUC = 0.6193, $P = 0.016$) and urinary hydroquinone (AUC = 0.6866, $P = 0.002$). ROC curve analyses were used for metabolic characterization in RE/SARE patients, and the differences were considered significant when the P value was ≤0.05.).

Table 2
Correlation analysis between clinical factors and characteristic metabolite.

		Pathology	Para-aortic RT	Surgery	CRRT	Risk level	FIGO Stage	Baseline SCC expression	Positive pelvic lymph node	Age	aCCI
Urine	Hydroquinone	0.007	0.622	0.916	0.610	0.878	0.270	0.328	0.754	0.748	0.748
Serum	AA	0.184	0.065	0.367	0.001	0.172	0.020	0.225	0.066	0.978	0.978
Serum	Fumaric acid	0.470	0.158	0.475	0.210	0.247	0.721	0.395	0.950	0.117	0.117
Fecal	Phenethylamine	0.718	0.000	0.017	0.852	0.076	0.615	0.839	0.249	0.476	0.476

AA: Arachidonic acid; FIGO: The International Federation of Gynecology and Obstetrics; SCC: squamous cell carcinoma; RT: radiotherapy; CRRT: concurrent chemoradiotherapy; aCCI: age-adjusted Charlson Comorbidity Index.

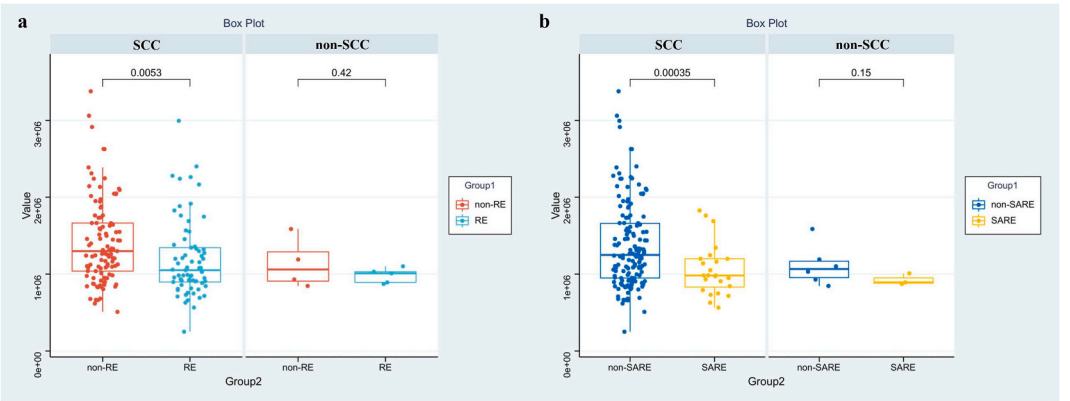

Fig. 4. Subgroup analysis of urinary hydroquinone (a–b: analysis of different pathologies. Significant differences in clinical characteristics were evaluated with Pearson's Chi-square test; differences were considered significant when the P value was ≤0.05.).

could help assess disease progression and the effectiveness of treatment strategies.

Subgroup analysis revealed that the expression of pyrocatechol in urine was significantly lower in patients who developed RE and SARE than in those who did not develop RE and SARE ($P < 0.05$ for both) among patients with SCC cervical cancer (Fig. 4a and b). Among those who developed RE and SARE (Fig. 4c and d), the expression of pyrocatechol in urine was significantly higher in patients with SCC than in those without SCC ($P < 0.01$). This suggests that urinary pyrocatechol levels could serve as a potential biomarker for predicting the risk or presence of RE and SARE in these patients. Furthermore, among the patients who developed RE or SARE, those with SCC had significantly higher levels of urinary pyrocatechol than those without SCC, indicating a potential association between specific cancer subtypes and metabolic responses to radiation therapy.

These findings underscore the importance of integrating metabolomics with clinical data for a more comprehensive understanding of cervical cancer. They highlight the potential of metabolic profiling in predicting treatment responses, managing complications like RE and SARE, and tailoring personalized treatment plans.

3.6. Metabolomics-based RE-SOM predictive classification model

We use mini-SOM library as an example, including 13 characteristic molecules mentioned earlier, such as phenethylamine, 4-hydroxyproline, fumaric acid, spermine, urine pyrocatechol, cytosine, N-acetyl-L-phenylalanine, fumaric acid, serum AA, fecal LC, AA, L-phenylalanine, and creatine, to establish a metabolic classification model for predicting RE and SARE.

We successfully established an effective RE mini-SOM classification model (Fig. 5A). The mapping plot in Fig. 5Aa shows that the separating line divides the enrolled data into two clusters, thus indicating a satisfactory classification effect. In terms of RE outcome classification (Fig. 5Ab-d), the group on the right side of the separating line represents RE patients, who are characterized by increased levels of spermine, urinary benzene diol, fecal AA, cytosine, fumarate, serum AA, and creatine. Conversely, the group on the left side of the separating line represents non-RE patients, who are characterized by increased levels of fecal LC, serum fumarate, N-acetyl-L-phenylalanine, phenethylamine, urinary 4-hydroxyproline, and L-phenylalanine. Based on metabolomics analysis, these results can be used as a classification model for RE.

This study successfully established an effective RE mini-SOM classification model. The model's ability to divide the enrolled data into two distinct clusters, as shown in the mapping plot, indicates its satisfactory classification effect. Clinically, this model can be immensely useful for identifying patients at risk of developing RE. By analyzing increased levels of specific metabolites like spermine, urinary benzene diol, fecal AA, and others, healthcare professionals can better predict and potentially prevent RE in patients undergoing radiation therapy. The study's findings differentiate RE patients, characterized by increased levels of certain metabolites, from non-RE patients, who show increased levels of different metabolites, such as fecal LC, serum fumarate, and others. This distinction is crucial for tailoring personalized interventions and monitoring strategies based on individual metabolic profiles, thus improving patient outcomes.

However, owing to the mediocre prediction classification of SARE-SOM based on metabolomics, the results cannot yet be

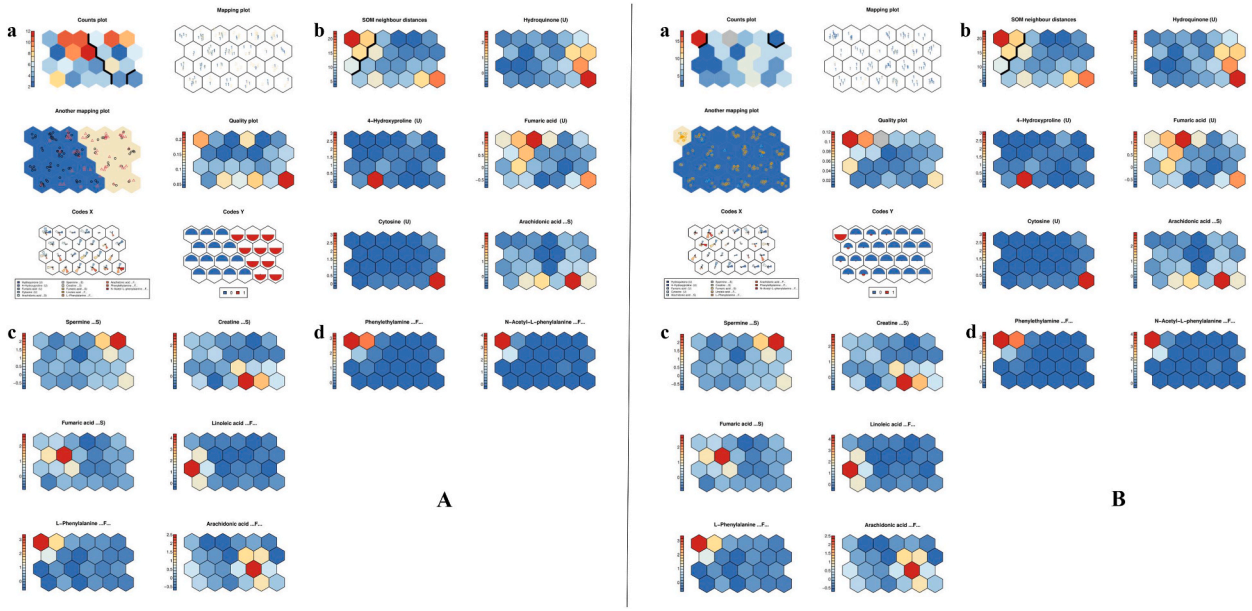

Fig. 5. A: Examples of RE's SOM model (a: min-SOM model U-Matrix and pie chart, b–d: component plane); B: examples of SARE's SOM model (a: min-SOM model U-Matrix and pie chart, b–d: component plane). Self-organizing maps (SOM) were used to predict metabolic molecule classification models for RE and SARE. The heatmaps were used to visualize the differences. The larger was the value, the darker is the color. (For interpretation of the references to color in this figure legend, the reader is referred to the Web version of this article.)

considered as a successful classification model (Fig. 5B). From the mapping plot, it can be seen that the entered data are divided into two clusters on the left and right sides of the line, and the classification effect is unsatisfactory (Fig. 5B). In terms of SARE outcome classification (Fig. 5Bb-d), the group on the left side of the separating line represents SARE patients, who are characterized by increased levels of fecal phenylethylamine, L-phenylalanine, and N-acetyl-L-phenylalanine. Conversely, the group on the right side of the separating line represents non-RE patients, who are characterized by increased levels of serum AA, spermine, creatine, fumaric acid, urinary quinone, 4-hydroxyproline, fumaric acid, cytosine, and fecal LC. The results cannot yet be used as an SARE classification model based on metabolomic analysis.

The SARE-SOM model based on metabolomics showed mediocre predictive performance. This indicates the complexity of predicting SARE and suggests that further refinement of the model is needed. The current results, showing different metabolic profiles for SARE and non-SARE patients, provide a foundation but are not reliable enough for clinical application. The study underscores the need for further research to improve the accuracy and reliability of metabolomics-based models for predicting SARE. Enhancing these models will be critical for their clinical adoption, allowing for early identification and management of SARE in patients.

4. Discussion

The occurrence and development of RE rely on the "co-metabolism" microenvironment formed by the composition of the host-gut microbiota and are affected by complex and strongly correlated influencing factors [10–12]. It is difficult to fully elucidate the mechanisms involved using conventional techniques. However, metabolomics analysis is a systems biology-based approach and offers many advantages in resolving the abovementioned problems. Its major advantages are as follows: (1) capable of dynamically analyzing the overall composition of metabolites, including feces, urine, blood, and secretions and cells of the body; (2) high accuracy, high sensitivity, and high throughput; and (3) based on multivariate statistical analysis methods, it can intuitively illustrate the pathological and physiological status of the research object, environmental factors, and the relationships between various groups of information, and obtain biomarkers [13,14]. This approach can explain the basic form of gut microbial metabolism and more accurately analyze the metabolic system, and consequently, the results obtained with this approach can help study the relationship between gut microbiota and the host [15–17].

Under steady-state conditions, the single-layered intestinal epithelial cells provide an effective chemical, physical, and charge barrier against luminal microbiota as well as other external factors. The epithelial defense mechanism primarily has three key components: pre-epithelial defense, epithelial defense, and post-epithelial defense (represented by the lamina propria) [18]. Furthermore, the pre-epithelial mucus barrier comprises mucins, which are lipids and proteins that form a continuous gel. The bicarbonate-rich liquid is secreted into the mucus, and it helps maintain neutral pH at the surface of the epithelium. Under conditions of compromised epithelial integrity, luminal antigens, such as pathogens, invade the subepithelial space, thereby sustaining and/or activating dysregulated inflammatory responses [19]. Inflammation triggers inflammatory chemokine synthesis, and numerous neutrophils flow into the tissue within hours of the injury [20]. In addition, the mucosal environment has an abundance of AA metabolites, inflammatory cytokines, and several other pro-inflammatory mediators during the acute phase of the inflammatory response, and this can activate the recruited leukocytes [21]. Notably, AA primarily exists as a membrane phospholipid component in most cells. Various cell or extracellular factors activate phospholipase, particularly phospholipase A2, to release AA from phospholipids [22]. Conversely, LC is a polyunsaturated fatty acid commonly found in plant oils, seeds, and nuts; it is also a membrane phospholipid component that acts as a structural component to maintain skin barrier function and can cause damage to hemoglobin and red blood cells through oxidative reactions [23]. In fecal samples, we found that the LC level increased in a time- and dose-dependent manner, whereas both fecal and serum samples showed initial decline followed by an increase in the AA level, which indicates the temporal sequence of LC and AA involvement in the cascade reaction of RE. Meanwhile, ROC curve analysis revealed AA as a predictor of RE, suggesting that AA has high specificity and sensitivity in reflecting RE occurrence. This suggests that the release of lipid components and the damage to cell membranes are the characteristics of RE after radiation exposure to the intestinal mucosa.

Aromatic amino acid (AAA) levels are reportedly associated with gut microbiota dysbiosis [24,25]. Using a mouse antibiotic model, Zhu et al. [26] found that long-term antibiotic intervention reduced *Roseburia* spp., *Clostridium* spp., *Lactobacillus* spp., and *Ruminococcus* spp. and increased *Bacteroides* spp., which adversely affected the metabolism of phenylalanine into phenylacetate, benzoate, phenylpropionate, and 4-hydroxybenzoate, thus increasing phenylalanine levels and subsequently leading to inflammation and immune system disorder. In this study, we found that in patients with cervical cancer undergoing VMAT alongside radiotherapy, N-acetyl-L-phenylalanine, phenylethylamine, and L-phenylalanine were significantly upregulated in a time- and dose-dependent manner in the phenylalanine metabolism pathway. Among them, phenylethylamine levels in feces had a certain predictive value for SARE, which was considered to be associated with the initiation and escalation of radiation-induced intestinal inflammation response and provided additional evidence for the researchers' conclusion from another perspective.

Notably, fumaric acid is involved upstream of arginine synthesis in the arginine and proline metabolism pathway. In this study, we also found that fumaric acid was first upregulated and then downregulated and had predictive value for SARE. 4-Hydroxyproline is involved downstream of arginine metabolism, and it showed a trend similar to that of fumaric acid; however, spermine and creatine levels showed decline in a time- and dose-dependent manner. The primary role of nitric oxide synthase (NOS) is catalysis of NADPH-dependent L-arginine and O_2 to provide NO and citrulline. However, all isoforms of NOS also produce superoxide (O_2^-) [27], forming neuronal (nNOS, NOS-1) and inducing (iNOS, NOS-2) to produce O_2- continuously, the latter of which consumes L-arginine as the main product [28]. NOS is stimulated to produce NO by ionizing radiation, thus causing temporary depletion of L-arginine in some microenvironments; this results in increased O_2^- production which cannot be effectively cleared by endogenous superoxide dismutase (SOD). Excessive O_2^- rapidly reacts to induce the production of residual and temporary aggregates of NO or continues to synthesize it in

other microenvironments, leading to the generation of destructive peroxynitrite. Herein, we also identified the "starvation" effect of arginine which was induced by ionizing radiation; this effect is associated with the initiation and amplification of RE and also embodies the body's self-regulatory process. Prophylactic use of L-arginine can reportedly alleviate radiation-induced immune dysfunction [29] and inflammation [30], and Jelonek et al. [31] reported that L-arginine can be used to protect hematopoietic stem cells from radiation. The findings of the present study also suggest intervention in arginine metabolism pathways as a new strategy for radiation protection in RE.

Ma et al. [32] investigated the antibacterial activity of hydroquinone against extensively drug-resistant, beta-lactamase-producing *Staphylococcus aureus*, methicillin-resistant *S. aureus*, and *S. aureus*. The antibacterial mechanism of hydroquinone was studied using bacterial extracellular protein leakage, alkaline phosphatase assay, and transmission electron microscopy. The findings revealed that hydroquinone had the ability to disrupt bacterial cell wall and membrane, increase bacterial cell wall and membrane permeability, affect protein synthesis, and lead to leakage of intracellular substances, such as alkaline phosphatase, inorganic ions, and soluble proteins. We herein found that hydroquinone in urine decreased in a time- and dose-dependent manner and could predict RE and SARE. The downregulation of hydroquinone results in antibacterial ability against Gram-positive bacteria, indirectly indicating that radiation induced the impairment of gut microbiota barrier function.

In recent years, accumulating evidence has shown that probiotic supplementation or reverse microbial reconstruction can be used to prove the metabolic pathways and mechanisms of intestinal flora in radiation injury. Ehrlich et al. [33] confirmed that *Bifidobacterium infantis* produces indole-3-lactic acid and protects cultured intestinal endothelial cells (IEC) by activating aryl hydrogen receptors and nuclear factor erythroid 2-related factor 2. Fecal microbiota transplantation (FMT) is a treatment method that reconstructs the patient's intestinal microbiota by isolating the intestinal flora of healthy people and transplanting it into the patient's intestine [34,35]. Xiao et al. [36] found in animal studies that FMT could increase the level of microbial-derived indole-3-propionic acid in the feces of irradiated mice, thus reducing systemic inflammation levels, reducing hematopoietic organ damage, relieving bone marrow suppression, and improving gastrointestinal function and maintain the integrity of the IEC. In the NCT03516461 clinical study, diarrhea, rectal bleeding, abdominal/rectal pain, and fecal incontinence improved in 3 of 5 patients with radiation enteritis, and 16S rRNA sequencing showed that FMT changed the composition of the patients' intestinal microbiota. This study demonstrates for the first time that FMT may be safe and effective in resolving intestinal symptoms and mucosal damage over a period of time in patients with chronic radiation enteritis [37]. In previous studies, we have identified characteristic bacterial groups related to acute RE. The above two methods provide effective research design ideas for subsequent intervention trials.

In a process-oriented study of VMAT for RE in patients with cervical cancer, we started from three common human biosamples and conducted liquid chromatography/mass spectrometry-based non-targeted metabolomics clustering and enrichment analyses of co-metabolic pathways. We found that in non-invasive biosamples, urine samples revealed initial upregulation followed by downregulation of arginine and proline metabolism pathway and arginine biosynthesis pathway; furthermore, these samples revealed downregulation of the pyrimidine and riboflavin metabolism pathways. Fecal supernatant revealed upregulation of LC-related metabolic pathways and phenylalanine metabolism, and it also revealed characteristic downregulation followed by upregulation of the amino acid metabolism pathway. Upon invasive peripheral venous blood sampling, serum samples revealed initial upregulation followed by downregulation of the arginine biosynthesis pathway as well as the downregulation of the arginine and proline metabolism pathway, glutathione metabolism pathway, and amino acid metabolism pathway. Subsequently, we identified the metabolic molecules that are predictive of RE (urinary benzene diol and serum amino acids) and SARE (fecal phenethylamine, urinary benzene diol, and serum fumaric acid). In addition, we established an effective RE mini-SOM classification model. Based on the above research results, we have preliminarily drawn the metabolic profile of intestinal bacteria co-metabolism associated with RE and SARE in patients undergoing VMAT for cervical cancer.

5. Conclusion

Patients with cervical cancer had characteristic metabolic pathways. The characteristic metabolites predictive of RE and SARE were successfully screened out. Preliminary outlines of the gut microbiota co-metabolism in RE and SARE environments were drawn in patients while they were undergoing VMAT for cervical cancer.

Ethics approval and consent to participate

This study was approved by the medical ethics committee of The First Affiliated Hospital of Soochow University [approval No. 2016 (100)]. All procedures performed in studies involving human participants were in accordance with the ethical standards of the institutional and/or national research committee and with the 1964 Helsinki declaration and its later amendments or comparable ethical standards. Signed informed consent was obtained from all participants.

Consent for publication

Not applicable.

Availability of data and materials

Data related to this study have been uploaded to China National Center for Bioinformation (https://ngdc.cncb.ac.cn/gsa-human/

submit/hra/submit).

Funding

This work was supported by the National Natural Science Foundation of China, China (No. 81602792), the Natural Science Foundation of the Jiangsu Higher Education Institutions of China (No. 23KJB310023), the Research Project of Maternal and Child Health in Jiangsu Province,China (No. F202210), the Jiangsu Provincial Medical Key Discipline (No. ZDXK202235), the Project of State Key Laboratory of Radiation Medicine and Protection, Soochow University (No. GZK1202101), the Suzhou Science and Technology Project, Grant/Award Number (No. SLT201920), the Suzhou Science and Technology Development, China Plan Project, Grant/Award Number (No. KJXW2020008), the BOXI Natural Science Cultivation Foundation of China of the First Affiliated Hospital of Soochow University (No. BXQN202107), and the Zhongguancun Precision Medicine Foundation's Medical and Health Public Welfare Initiative (No. XS-ZGC-0012). The authors declare that they have no financial relationship with the organization that sponsored the research, and the funding body was not involved in study design, data collection, analysis and writing of the study.

CRediT authorship contribution statement

Chen-ying Ma: Writing – review & editing, Validation, Investigation, Data curation, Conceptualization. **Jing Zhao:** Writing – original draft, Supervision, Project administration, Formal analysis, Conceptualization. **Ju-ying Zhou:** Writing – review & editing, Project administration, Funding acquisition, Conceptualization.

Declaration of competing interest

The authors declare that they have no known competing financial interests or personal relationships that could have appeared to influence the work reported in this paper.

Acknowledgements

Not applicable.

List of Abbreviations

RE	radiation enteritis
SARE	severe acute radiation enteritis
VMAT	volumetric modulated arc therapy
SARE-SS	severe acute radiation enteritis scoring system
FIGO	The International Federation of Gynecology and Obstetrics
CT	Computed Tomography
ROC curve	receiver operating characteristic curve
AUC	area under the ROC curve
CTCAE	National Institutes of Health Common Adverse Events Evaluation Criteria
OPLS-DA	orthogonal partial least squares discriminant analysis
SOM	self-organizing maps
LC	linoleic acid
AA	arachidonic acid
AAAs	aromatic amino acids
NOS	nitric oxide synthase
SOD	superoxide dismutase
SCC	squamous cell carcinoma
non-SCC	non-squamous cell carcinoma
RT	radiotherapy
CRRT	concurrent chemoradiotherapy
aCCI	age-adjusted Charlson Comorbidity Index
PCoA	principal co-ordinates analysis
CID	collision-induced dissociation
VIP	variable importance for the projection

References

[1] N. Guo, M. Liu, Z. Yang, et al., The synergistic mechanism of β-lactam antibiotic removal between ammonia-oxidizing microorganisms and heterotrophs, Environ. Res. 216 (2023) 114419. https://doi:10.1016/j.envres.2022.114419.

[2] G. Al-Qadami, G. Verma, Y. Van Sebille, et al., Antibiotic-induced gut microbiota depletion accelerates the recovery of radiation-induced oral mucositis in rats, Int. J. Radiat. Oncol. Biol. Phys. 113 (2022) 845–858, https://doi.org/10.1016/j.ijrobp.2022.03.036.

[3] A.G. Cheng, P.Y. Ho, A. Aranda-Díaz, et al., Design, construction, and in vivo augmentation of a complex gut microbiome, Cell 185 (2022) 3617–3636.e19. https://doi:10.1016/j.cell.2022.08.003.

[4] V.K. Singh, O.O. Fatanmi, S.Y. Wise, et al., Novel biomarkers for acute radiation injury and countermeasures using large and small animal models and multi-omics approach, Radiat Prot Dosimetry 199 (2023) 1526–1532. https://doi:10.1093/rpd/ncad035.

[5] Y. Li, L. Sui, H. Zhao, et al., Differences in the establishment of gut microbiota and metabolome characteristics between balb/c and C57BL/6J mice after proton irradiation, Front. Microbiol. 13 (2022) 874702. https://doi:10.3389/fmicb.2022.874702.

[6] L.C. Soares, R.J. de Souza, M.A.P. Oliveira, Reviewing FIGO 2018 cervical cancer staging, Acta Obstet. Gynecol. Scand. 102 (2023) 1757–1758. https://doi:10.1111/aogs.14667.

[7] L. Kumar, A. Upadhyay, A.S. Jayaraj, Chemotherapy and immune check point inhibitors in the management of cervical cancer, Curr. Probl. Cancer 46 (2022) 100900. https://doi:10.1016/j.currproblcancer.2022.100900.

[8] C. Chen, X. Meng, Y. Zhu, et al., Early identification of serum biomarkers and pathways of sepsis through GC-MS-based metabolomics analysis, Front Biosci (Landmark Ed) 28 (2023) 145. https://doi:10.31083/j.fbl2807145.

[9] J.J. Mohsen, A.A. Martel, et al., Microproteins-Discovery, structure, and function, Proteomics 23 (2023) e2100211. https://doi:10.1002/pmic.202100211.

[10] Y. Cui, H. Wu, Z. Liu, et al., CXCL16 inhibits epithelial regeneration and promotes fibrosis during the progression of radiation enteritis, J. Pathol. 259 (2023) 180–193. https://doi:10.1002/path.6031.

[11] K.Y. He, X.Y. Lei, D.H. Wu, et al., Akkermansia muciniphila protects the intestine from irradiation-induced injury by secretion of propionic acid, Gut Microb. 15 (2023) 2293312. https://doi:10.1080/19490976.2023.2293312.

[12] S.U. Lee, B.S. Jang, Y.R. Na, et al., Effect of Lactobacillus rhamnosus GG for regulation of inflammatory response in radiation-induced enteritis, Probiotics Antimicrob Proteins 16 (2024) 636–648. https://doi:10.1007/s12602-023-10071-9.

[13] S. Pal, D. Rendedula, N. Kumar Nagendla, et al., Serum and urine metabolomics analysis reveals the role of altered metabolites in patulin-induced nephrotoxicity, Food Res. Int. 156 (2022) 111177, https://doi.org/10.1016/j.foodres.2022.111177.

[14] F. Li, Y. Pi, M. Zhang, et al., Urine and serum metabolomics study of wild ginseng in rats with spleen-qi deficiency using rapid resolution liquid chromatography coupled with quadrupole-time-of-flight mass spectrometry, J Sep Sci 46 (2023) e2300344, https://doi.org/10.1002/jssc.202300344.

[15] H. Pelantová, P. Tomášová, B. Šedivá, et al., Metabolomic study of aging in fa/fa rats: multiplatform urine and serum analysis, Metabolites 13 (2023) 552, https://doi.org/10.3390/metabo13040552.

[16] S. Fromentin, S.K. Forslund, K. Chechi, et al., Microbiome and metabolome features of the cardiometabolic disease spectrum, Nat Med 28 (2022) 303–314, https://doi.org/10.1038/s41591-022-01688-4.

[17] Y. Yu, X. Lin, F. Feng, et al., Gut microbiota and ionizing radiation-induced damage: is there a link? Environ. Res. 229 (2023) 115947 https://doi.org/10.1016/j.envres.2023.115947.

[18] W.M. de Vos, H. Tilg, M. Van Hul, et al., Gut microbiome and health: mechanistic insights, Gut 71 (2022) 1020–1032. https://doi:10.1136/gutjnl-2021-326789.

[19] Q. Shen, Z. Huang, J. Yao, Y. Jin, Extracellular vesicles-mediated interaction within intestinal microenvironment in inflammatory bowel disease, J. Adv. Res. 37 (2022) 221–233, https://doi.org/10.1016/j.jare.2021.07.002.

[20] Y. Haneishi, Y. Furuya, M. Hasegawa, et al., Inflammatory bowel diseases and gut microbiota, Int. J. Mol. Sci. 24 (2023) 3817. https://doi:10.3390/ijms24043817.

[21] L. Li, T. Liu, Y. Gu, et al., Regulation of gut microbiota-bile acids axis by probiotics in inflammatory bowel disease, Front Immunolv 13 (2022) 974305. https://doi:10.3389/fimmu.2022.974305.

[22] A. Mukherjee, A.J. Bilecz, E. Lengyel, The adipocyte microenvironment and cancer, Cancer Metastasis Rev. 41 (2022) 575–587.

[23] O. Asbaghi, G. Shimi, K. Naseri, et al., The effects of conjugated linoleic acid supplementation on blood pressure and endothelial function in adults: a systematic review and dose-response meta-analysis, Eur. J. Pharmacol. 931 (2022) 175162, https://doi.org/10.1016/j.ejphar.2022.175162.

[24] X. Su, Y. Gao, R. Yang, Gut microbiota-derived tryptophan metabolites maintain gut and systemic homeostasis, Cells 11 (2022) 2296. https://doi:10.3390/cells11152296.

[25] Y. Sugiyama, Y. Mori, M. Nara, et al., Gut bacterial aromatic amine production: aromatic amino acid decarboxylase and its effects on peripheral serotonin production, Gut Microb. 14 (2022) 2128605. https://doi:10.1080/19490976.2022.2128605.

[26] X. Zhu, B. Fu, M. Dong, et al., Effects of long-term antibiotic treatment on mice urinary aromatic amino acid profiles, Biosci. Rep. 41 (2021). BSR20203498, https://doi:10.1042/BSR20203498.

[27] E. Idrizaj, S. Nistri, V. Zizi, M.C. Baccari, Neuronal nitric oxide synthase as a shared target for the effects of adiponectin and resistin on the mechanical responses of the mouse gastric fundus, Int. J. Mol. Sci. 23 (2022), https://doi.org/10.3390/ijms232416113.

[28] K. Solanki, S. Rajpoot, E.E. Bezsonov, et al., The expanding roles of neuronal nitric oxide synthase (NOS1), PeerJ 10 (2022) e13651, https://doi.org/10.7717/peerj.13651.

[29] I.L.A.A. Martí, W. Reith, Arginine-dependent immune responses, Cell. Mol. Life Sci. 78 (2021) 5303–5324, https://doi.org/10.1007/s00018-021-03828-4.

[30] M. Liang, Z. Wang, H. Li, B. Liu, L. Yang, l-Arginine prevents 4-hydroxy-2-nonenal accumulation and depresses inflammation via inhibiting NF-κB activation, J. Biochem. Mol. Toxicol. 36 (2022) e23087, https://doi.org/10.1002/jbt.23087.

[31] K. Jelonek, K. Mrowiec, D. Gabryś, et al., The metabolic footprint of systemic effects in the blood caused by radiotherapy and inflammatory conditions: a systematic review, Metabolites 13 (2023) 1000. https://doi:10.3390/metabo13091000.

[32] C. Ma, N. He, Y. Zhao, D. Xia, J. Wei, W. Kang, Antimicrobial mechanism of hydroquinone, Appl. Biochem. Biotechnol. 189 (2019) 1291–1303, https://doi.org/10.1007/s12010-019-03067-1.

[33] A.M. Ehrlich, A.R. Pacheco, B.M. Henrick, et al., Indole-3-lactic acid associated with Bifidobacterium-dominated microbiota significantly decreases inflammation in intestinal epithelial cells, BMC Microbiol. 20 (2020) 357. https://doi:10.1186/s12866-020-02023-y.

[34] J. Liu, C. Liu, J. Yue, Radiotherapy and the gut microbiome: facts and fiction, Radiat. Oncol. 16 (2021) 9. https://doi:10.1186/s13014-020-01735-9.

[35] W. Wang, B. Cui, Y. Nie, et al., Radiation injury and gut microbiota-based treatment, Protein Cell 15 (2024) 83–97, in: https://doi:10.1093/procel/pwad044.

[36] H.W. Xiao, M. Cui, Y. Li, et al., Gut microbiota-derived indole 3-propionic acid protects against radiation toxicity via retaining acyl-CoA-binding protein, Microbiome 8 (2020) 69. https://doi:10.1186/s40168-020-00845-6.

[37] X. Ding, Q. Li, P. Li, et al., Fecal microbiota transplantation: a promising treatment for radiation enteritis? Radiother. Oncol. 143 (2020) 12–18. https://doi:10.1016/j.radonc.2020.01.011.